02

Luminescent characteristics of ZrHfYEuO ceramics

© E.V. Dementeva, A.A. Shakirova, P.A. Dementev, K.N. Orekhova, M.V. Zamoryanskaya

Ioffe Institute, St. Petersburg, Russia

e-mail: ivanova@mail.ioffe.ru

Received September 04, 2023
Revised August 24, 2023
Accepted September 25, 2023

Luminescent characteristics of $Zr_{0.38}Hf_{0.45}Y_{0.1}Eu_{0.07}O_{1.91}$ ceramics prepared by co-precipitation from a common solution followed by sintering and additional annealing in an argon atmosphere have been studied. It has been shown that ceramics have a cubic crystal structure. Annealing ceramics in an argon atmosphere leads to an increase in the luminescence intensity of Eu^{3+}. Based on the analysis of luminescence spectra of europium ion, it has been concluded that after annealing the Eu^{3+} ion occupies a more symmetrical position in the crystal lattice. The appearance of intense broad bands in the emission spectra allows us to conclude that during the annealing process in an argon atmosphere, diffusion of oxygen from the sample occurs, and the process of oxygen diffusion is more active in areas with small grain sizes.

Keywords: zirconium oxide, hafnium oxide, ceramics, cathodoluminescence, point defects, Eu^{3+} luminescence Eu^{3+}.

DOI: 10.61011/EOS.2023.10.57758.5619-23

Introduction

The ceramic materials are of great practical interest and applied in various field of science and technics. Recently, large attention is paid to studies of the ceramics based on zirconium and hafnium oxides in a cubic structural modification. In order to obtain the stable cubic phase, the ceramics should be stabilized by three-valence ions, for example, by ions of the rare earth elements (primarily, yttrium and similar lanthanides). Many studies have been devoted to investigating luminescent properties of the Y-stabilized ceramics based on ZrO_2 (YSZ), which is codoped by the ion oxides of the three-valence metals: Dy_2O_3 [1], Er_2O_3 [2], Eu_2O_3 [3,4]. There are still studies of the thermodynamic properties of this ceramics in connection of using YSZ as the thermal barrier coatings [5,6] and other applications [7]. One of the possible application of the ceramics based on the Y-stabilized ZrO_2 is development of ionizing radiation sensors based on the thermoluminescence phenomenon. In this regard, there is active discussion about specific features of the crystal structure and the electron structure of the charge carrier traps in these materials depending on doping or a ceramics production method [4]. Special interest of the studies includes thermoluminescent properties of the YSZ ceramics codoped with the various three-valence metals: Eu [8], Er [9], etc.

The studies in this field make it possible to develop radiation-resistant thermoluminescent dosimeters designed to measure high doses of ionising radiation. It should be also noted that the ceramics based on zirconium and hafnium dioxides activated by rare-earth ions and stabilized in the cubic phase, is of particular interest since the transparent ceramics can be potentially formed based thereon.

An important characteristic of the material for thermoluminescent dosimetry is high concentration of the traps with quite high activation energy for avoiding release of the charge carriers at the room temperature. There is extensive investigation of the traps in the thin films HfO_2 and $Hf_xZr_{x-1}O_2$ [10–13], but there are almost no such study for the bulk or ceramics samples. Some studies have shown that the traps in this material are connected with oxygen vacancies [14–16]. One of the ways for generating the oxygen vacancies is high-temperature annealing in a non-oxygen atmosphere. The present paper is devoted to studying the influence of high-temperature annealing of the $Zr_{0.41}Hf_{0.41}Y_{0.09}Eu_{0.09}O_{1.91}$ ceramics with a cubic crystal structure in the argon atmosphere on its luminescent properties.

Sample synthesis and study methods

Thethe sample of the ZrHfYEuO ceramics with the content of yttrium and europium about 9% at. was synthesized, since such concentration of the three-valence elements reliably stabilizes the zirconium and hafnium oxides in the cubic phase [17]. For synthesis of a charge material, co-precipitation from a common solution was selected as it is the most promising, economically expedient and acceptable for industrial implementation. Then the charge materials were ground and pressed into tablets with a diameter of 8 mm under a pressure of 10 MPa. The obtained tablets were sintered in air at the temperature of 1500°C for 3 h. Then, one of the samples was additionally annealed in the argon atmosphere at the temperature of 1500°C for 3 h. Both samples were sawn, fixed in epoxy resin and their surface was covered with a carbon film to provide electron drain.

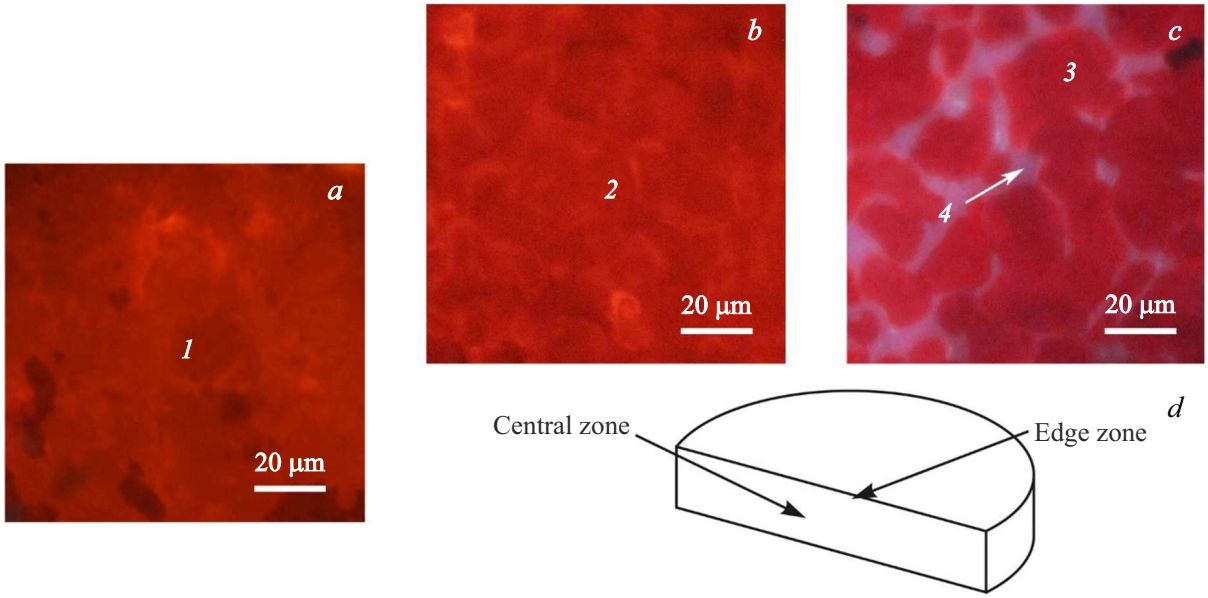

Figure 1. CL-images (a) of the initial ZrHfYEuO ceramics, (b) the ZrHfYEuO ceramics after annealing in a central area of the sample in the argon atmosphere, (c) the ZrHfYEuO ceramics after annealing in the edge area of the sample in the argon atmosphere, (d) a conditional diagram designating a position of the central and the edge areas on a sawcut plane of the tables. The digits of the images indicate points of subsequent measurements of the CL spectra and the dynamics of luminescence decay.

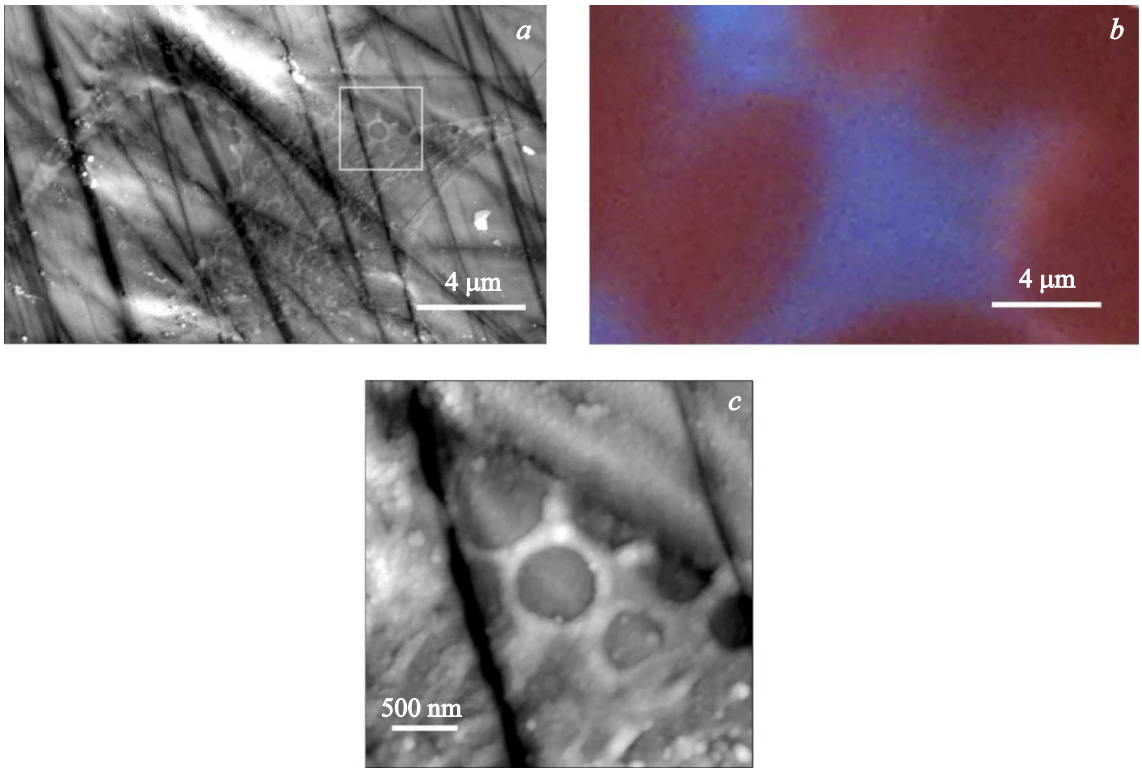

Figure 2. (a) AFM-image of the area $20 \times 12\,\mu$m. The full vertical drop is 115 nm; (b) a cut-of part of the CL image (Fig. 1, c), which corresponds to the AFM image; (c) the enlarged AFM image (it is shown by a square on Fig. a). The full vertical drop is 56 nm.

The elemental composition of the studied samples was obtained by electron microprobe analysis (EMPA). The composition was studied on a CAMEBAX electron probe microanalyzer equipped with four X-ray spectrometers, with the following electron beam parameters: the energy $U = 20$ keV, the absorbed current $I = 15$ nA, the beam

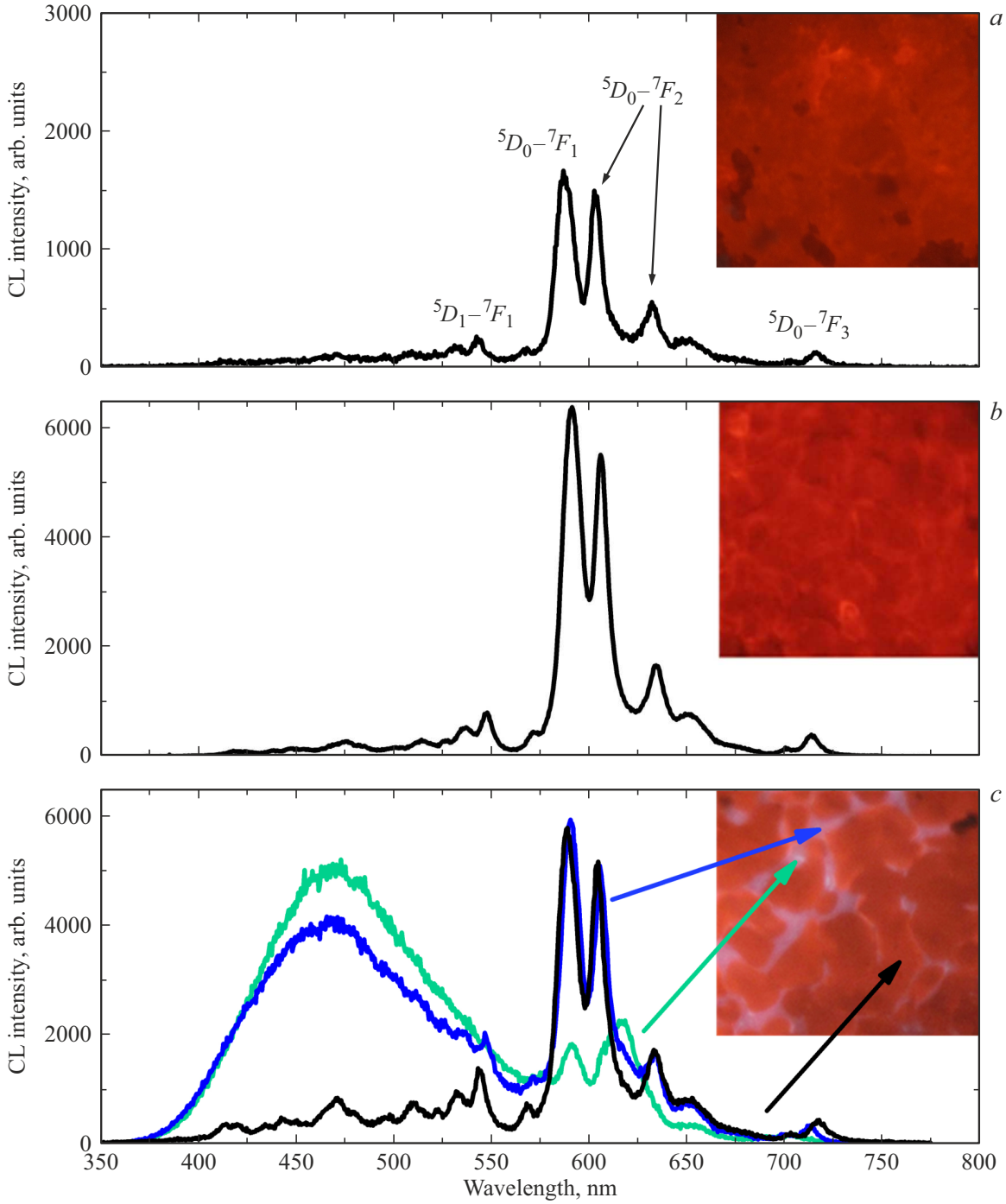

Figure 3. CL-images and spectra (a) of the initial ZrHfYEuO ceramics (Fig. 1, a); (b) the ZrHfYEuO ceramics after annealing in the central area in the argon atmosphere (Fig. 1, b); (c) the ZrHfYEuO after annealing in the edge area in the argon atmosphere (Fig. 1, c).

diameter $d = 2\,\mu$m. For analysis, the analytical line Lα was chosen for all the elements. The standards selected included metallic zirconium (for determination of Zr), metallic hafnium (for Hf), the compounds $Y_3Al_5O_{12}$ (for Y) and $EuPO_4$ (for Eu). The oxygen content was calculated based on stoichiometry. The elemental composition was measured in several (minimum five) randomly selected areas of the samples and then averaged.

The luminescent properties of a concentration series of samples were studied by cathodoluminescence (CL) using the same CAMEBAX setup, additionally equipped with an optical spectrometer [10]. The spectra of the CL samples were obtained within the wavelength range of $\lambda = 350-800$ nm: the electron beam energy $U = 20$ keV, the absorbed current $I = 50$ nA and the beam diameter $d = 5\,\mu$m. CL images of the samples were obtained

under the following conditions: electron beam energy $U = 20\,\text{keV}$, absorbed current $I = 100\,\text{nA}$, and beam diameter $d = 200\,\mu\text{m}$.

The surface relief was studied using an NTegra-Aura atomic-force microscopy (NTMDT-SI, Moscow, Russia) by means of standard silicon probes (the rigidity $\sim 4\,\text{N/m}$, the typical radius of the probe tip rounding $\sim 10\,\text{nm}$). The measurements were done in a semi-contact mode in air.

Results

The EMPA has shown that the average elemental composition of the ceramics was — $Zr_{0.38}Hf_{0.45}Y_{0.1}Eu_{0.07}O_{1.91}$. A deviation from the planned composition does not exceed error limits of the measurement method (10% for europium; 2% for other elements in the samples [18]).

The optical microscopy and CL images were obtained for initial and annealed samples (Fig. 1). The optical images of the initial samples (omitted in the article) show a contrast related to the surface topography. The dark areas in CL images match the contrast in optical images, suggesting that the contrast in CL images is also related to the surface topography of the samples. The additional EMPA studies have shown that this contrast was not related to fluctuations of the composition within the method accuracy.

The ceramics annealed in the argon atmosphere can have two areas distinguished: the central area and the edge area. Fig. 1, *b* and Fig. 1, *c* show the corresponding CL images. For better understanding, Fig. 1, *d* shows the conditional diagram of the position of the areas for obtaining the CL images and the spectra on the table sawcut surface. Blue inclusions are observed in the CL images of the edge areas. The size of the annealed sample's area exhibiting the blue inclusions is approximately $500\,\mu\text{m}$. In order to clarify the causes of origin of the blue inclusions, the sample surface relief was subjected to AFM study. The results obtained are shown on Fig. 2. Fig. 2, *a* shows the image of the surface area of a size of $20 \times 12\,\mu\text{m}$. Deep traces due to surface machining are well visible. In addition, it can be noted that this surface portion exhibits areas of the two types — the smooth one and the microrelief one. One of such areas (marked with a square) has been studied in detail (Fig. 2, *c*). It is evident that the microrelief is a set of grains with well discernable boundaries with a typical size about 500 nm. A right top corner of this image also exhibits a smooth area, in which, indeed, no such specific features are observed. By the typical specific features, the studied place was identified on the CL image (Fig. 1, *c*), and an area, which exactly matched the AFM image, was cut. It is easy to note that the blue inclusions match the microrelief areas of the AFM image with high accuracy. Thus, it can be stated that blue luminescence is observed in the areas with the grain size about 500 nm.

The CL spectrum of the initial ceramics (Fig. 3, *a*) exhibits bands related to the transitions $^5D_1 - ^7F_1$ and $^5D_0 - ^7F_{0,1,2,3,4}$ Eu^{3+}. The ratio of the bands of the main transitions corresponds to the ratio of the bands in the cubic oxide of zirconium [19,20]. The CL spectra of the annealed sample (Fig. 3, *b, c*) also exhibits bands related to luminescence Eu^{3+}, but some areas of the sample have the CL bands ratio that is different from the ratio observed in the cubic phase. In accordance with paper [19], this peak ratio is typical of the inclusions of the monoclinic phase. Accordingly, it can be stated that the prevailing part of the ceramics remains int he cubic phase, but the inclusions of the monoclinic phase appear as well. The luminescence intensity of the annealed ceramics approximately by four times exceeds the intensity of the initial one. The CL spectra of the blue luminescence areas (Fig. 1, *c* and Fig. 3, *c*) exhibit a wide band in the blue spectrum range, which is related to luminescence of intrinsic defects. This band has an intensity maximum at 2.7 eV (470 nm) and a half-width of 0.5 eV and the band is associated with the oxygen vacancies in the main matrix [16,21]. It is interesting that the grains of red luminescence in the edge area (Fig. 1, *c*, the spot *3*) exhibits an increase in the intensity of the high-energy transitions Eu^{3+} from the levels $^5D_3$ and $^5D_1$, which can be related to increase in the intrinsic defects in this area and appearance of the wide band in this range. As it is shown on Fig. 2, the intensive blue luminescence is observed in the ceramics areas with a small grain size. Accordingly, it can be stated that the argon annealing process leads to oxygen diffusion out of the sample, wherein the diffusion is more active in the areas with the small grain size.

Luminescence decay times of the $^5D_0 - ^7F_1$ Eu^{3+} transition and the contributions of the exponents with the different indexes τ, obtained in the areas, are shown on Fig. 1.

Sample	Initial	After annealing		
№ of spot	1	2	3	4
A_1	0.49±0.02	0.44±0.02	0.44±0.02	0.44±0.02
τ_1, μs	625 ± 20	520 ± 20	615 ± 30	580 ± 20
A_2	0.51 ± 0.02	0.56 ± 0.02	0.56 ± 0.02	0.56 ± 0.02
τ_2, μs	40 ± 2	64 ± 5	60 ± 5	65 ± 5

The transition $^5D_0 - ^7F_1$ is a magnetic dipole (MD) transition and it weakly depends on the local neighboring of the ions Eu^{3+} unlike the electrodipole (ED) transition $^5D_0 - ^7F_2$. In the neighboring with inversion symmetry, the intensity of the ED transition $^5D_0 - ^7F_2$ drops due to parity prohibition and the MD transition $^5D_0 - ^7F_1$ becomes the most intensive in the luminescence spectrum [20]. The relationship $I_{(\text{ED})}/I_{(\text{MD})}$ is called an asymmetry factor, and the bigger it, the lower the symmetry of the local position occupied by Eu^{3+}. The asymmetry factor has been calculated as per the procedure proposed in the paper [20] and tested in the paper [23]. It is shown that the asymmetry factor of the initial sample is 1.21 ± 0.01, while in the

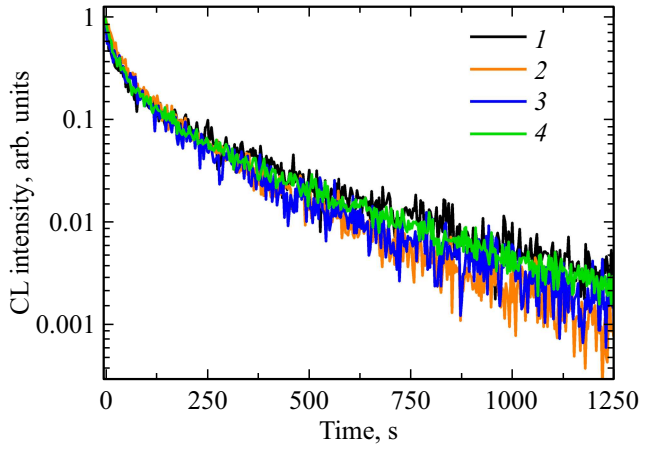

Figure 4. Decay dynamics curves for the transition Eu^{3+} $^5D_0 - ^7F_1$ in a semi-logarithmic scale, the spot *1*, and the annealed sample, the spots *2, 3* and *4*, which correspond to the spots in Fig. 1.

sample after annealing it is 1.180 ± 0.005 in all the studied areas.

The decay times of the band Eu^{3+} $^5D_0 - ^7F_1$ in the initial and annealed samples and of the band in the spectrum's blue range have been measured (Fig. 4). The decay dynamics curves of the transition Eu^{3+} $^5D_0 - ^7F_1$ are well approximated by the two exponents. The short decay component is usually associated with the centers near grain boundaries [22,23]. The results of approximation are listed in the table. It is evident that after annealing in argon the contribution of the short time is insignificantly increased, while the short time itself is lengthened in 1.5 times, wherein the times in the various areas of the sample match each other within the error limits. The long time is unchanged within the measurement errors. The increased time of decay and intensity of luminescence of the transition Eu^{3+} $^5D_0 - ^7F_1$ signifies that the additionally-annealed ceramics has a decreased number of the defects contributing to nonradiative recombination.

For all the samples, each obtained decay kinetics has been approximated by a sum of the two exponents:

$$I = I_0 + A_1 \exp\left(-\frac{t}{\tau_1}\right) + A_2 \exp\left(-\frac{t}{\tau_2}\right).$$

The parameters A_1 and A_2 provide information about the contribution of each exponent to the kinetics of luminescence decay, while the exponent powers τ_1 and τ_2 characterize the times of luminescence decay. The obtained values of the parameters are given in the table.

It also included the measurement of the decay kinetics of the wide band in the blue range, which is related to luminescence of the intrinsic defects. The dynamics of its decay is also approximated by the two exponents with the times $2.3 \pm 0.1\,\mu$s and $0.4 \pm 0.1\,\mu$s. It can be assumed that as well as for the europium ions, the shorter decay time is related to the centers near the boundaries.

Conclusions

It is evident from the above-given data that annealing in the argon atmosphere results in some changes in the structure and the optical properties of the ceramics. First, the content of the defects is decreased, which is expressed in the increased decay time and intensity of luminescence of Eu^{3+}. Secondly, there is reduction of the asymmetry factor observed after annealing, which signifies that the ion Eu^{3+} occupies a more symmetrical position. Thirdly, the areas with blue luminescence are visualized on the CL images. It is evident from the CL spectra that the color of the areas is related to appearance of the wide band with the maximum of 2.7 eV. The literature relates this band to the defects of oxygen deficiency. It can be stated that the process of annealing in the argon atmosphere leads to oxygen diffusion out of the sample, wherein the oxygen diffusion process is more active in the areas with the small grain size.

Funding

E.V. Dementieva, A.A. Shakirova, P.A. Dementiev, K.N. Orekhova would like to thank the Russian Science Foundation for the support (the project № 23-23-00465). https://rscf.ru/project/23-23-00465/.

Conflict of interest

The authors declare that they have no conflict of interest.

References

[1] X. Hong, S. Xu, X. Wang, D. Wang, S. Li, B.A. Goodman, W. Deng. J. Lumin., **231**, 117766 (2021). DOI: 10.1016/j.jlumin.2020.117766
[2] X. Wang, X. Tan, S. Xu, F. Liu, B.A. Goodman, W. Deng. J. Lumin., **219**, 116896 (2020). DOI: 10.1016/j.jlumin.2019.116896
[3] S. Stepanov, O. Khasanov, E. Dvilis, V. Paygin, D. Valiev, M. Ferrari. Ceram. Int., **47**, 6608 (2021). DOI: 10.1016/j.ceramint.2020.10.250
[4] M. Eibl, S. Shaw, D. Prieur, A. Rossberg, M.C. Wilding, C. Hennig, K. Morris, J. Rothe, T. Stumpf, N. Huittinen. J. Mater. Sci., **55**, 10095 (2020). DOI: 10.1007/s10853-020-04768-3
[5] L.J. Espinoza-Pérez, E. López-Honorato, L.A. González. Ceram. Int., **46** (10, Part A), 15621 (2020). DOI: 10.1016/j.ceramint.2020.03.109
[6] K.-J. Hwang, M. Shin, M.-H. Lee, H. Lee, M.Y. Oh, T.H. Shin. Ceram. Int., **45** (7, Part B), 9462 (2019). DOI: 10.1016/j.ceramint.2018.09.026
[7] A. Loganathan, A.S. Gandhi. J. Mater. Sci., **52**, 7199–7206 (2017). DOI: 10.1007/s10853-017-0956-2
[8] L. Yang, D. Peng, X. Shan, F. Guo, Y. Liu, X. Zhao, P. Xiao. Sens. Actuators B Chem., **254**, 578 (2018). DOI: 10.1016/j.snb.2017.07.092
[9] H.S. Lokesha, M.L. Chithambo. Radiat. Phys. Chem., **172**, 108767 (2020). DOI: 10.1016/j.radphyschem.2020.108767

[10] C. Zhao, C. Zhou Zhao, S. Taylor, P.R. Chalker. Materials, **7**, 5117 (2014). DOI: 10.3390/ma7075117
[11] V.A. Gritsenko, T.V. Perevalov, D.R. Islamov. Phys. Rep., **613**, 1 (2016). DOI: 10.1016/j.physrep.2015.11.002
[12] E.J. Shin, S.W. Shin, S.H. Lee, T.I. Lee, M.J. Kim, H.J. Ahn, J.H. Kim, W.S. Hwang, J. Lee, B.J. Cho. IEEE International Electron Devices Meeting (IEDM), 6.2.1 (2020). DOI: 10.1109/IEDM13553.2020.9371984.
[13] C. Jin, C.J. Su, Y.J. Lee, P.J. Sung, T. Hiramoto, M. Kobayashi. IEEE Trans Electron Devices, **68** (3), 1304 (2021). DOI: 10.1109/TED.2020.3048916
[14] T.V. Perevalov, D.V. Gulyaev, V.S. Aliev, K.S. Zhuravlev, V.A. Gritsenko, A.P. Yelisseyev. J. Appl. Phys., **116**, 244109 (2014). DOI: 10.1063/1.4905105
[15] D.R. Islamov, V.A. Gritsenko, T.V. Perevalov, V.Sh. Aliev, V.A. Nadolinny, A. Chin. Materialia, **15**, 100980 (2021). DOI: 10.1016/j.mtla.2020.100980
[16] E.V. Dementeva, P.A. Dementev, M.A. Yagovkina, M.V. Zamoryanskaya. ACS Appl. Nano Mater., **6** (18), 16212 (2023). DOI: 10.1021/acsanm.3c02178
[17] J. Dexpert-Ghys, M. Faucher, P. Caro. J. Solid State Chem., **54** (2), 179 (1984). DOI: 10.1016/0022-4596(84)90145-2
[18] G.A. Gusev, S.M. Masloboeva, M.A. Yagovkina, M.V. Zamoryanskaya. Opt. Spectrosc., **130** (2), 265 (2022). DOI: 10.61011/EOS.2023.10.57758.5619-23
[19] E.V. Ivanova, V.A. Kravets, K.N. Orekhova, G.A. Gusev, T.B. Popova, M.A. Yagovkina, O.G. Bogdanova, B.E. Burakov, M.V. Zamoryanskaya, J. Alloy. Compd., **808**, 151778 (2019). DOI: 10.1016/j.jallcom.2019.151778
[20] V.A. Kravets, K.N. Orekhova, M.A. Yagovkina, E.V. Ivanova, M.V. Zamoryanskaya. Opt. Spectrosc., **125**, 188 (2018). DOI: 10.1134/S0030400X18080167.
[21] E.V. Dementeva, M.V. Zamoryanskaya, V.A. Gritsenko. Opt. Spectrosc., **130** (12), 1563 (2022). DOI: 10.61011/EOS.2023.10.57758.5619-23
[22] A.A. Shakirova, E.V. Dementieva, T.B. Popova, M.V. Zamoryanskaya. Opt. i spektr., **131** (5), 10 (2023) (in Russian). DOI: 10.61011/EOS.2023.10.57758.5619-23
[23] K. Orekhova, M. Zamoryanskaya. J. Lumin., **251**, 119228 (2022). DOI: 10.1016/j.jlumin.2022.119228

Translated by M.Shevelev